Alexa 546-conjugated goat antibodies to mouse or rabbit IgG were obtained from Molecular Probes. Antibodies were used at a dilution of 1:2,000.

Plasmids. Complementary DNAs encoding wild-type or mutant forms of mouse $CHD8_S$ or human $CHD8_L$, each tagged at its N terminus with Flag, Myc or HA epitopes, were subcloned into pcDNA3 (Invitrogen). Complementary DNAs encoding wild-type or mutant forms of human p53, each tagged at its N terminus with the HA epitope, were subcloned into pCGN. Complementary DNAs encoding mouse histone H1 variants, each tagged at its N terminus with three copies of the Flag epitope, were subcloned into pcDNA3. His_6-tagged proteins were expressed in *Escherichia coli* strain BL21(DE3)pLys(S) (Novagen).

Cell culture, transfection and infection. HEK293T, HeLa, HCT116, U2OS and SaOS2 cells were cultured in an atmosphere of 5% CO_2 at 37°C in Dulbecco's modified Eagle's medium (DMEM, Invitrogen) supplemented with 10% fetal bovine serum (Invitrogen). NIH 3T3 cells were cultured under the same conditions in DMEM supplemented with 10% bovine serum (Invitrogen). MEFs and ES cells were cultured as described previously[41,42]. HEK293T, HeLa and SaOS2 cells were transfected with vectors using FuGENE6 (Roche). For retroviral infection, cDNAs were subcloned into pMX-puro.

Immunoprecipitation and immunoblot analysis. Cell lysis, immunoprecipitation and immunoblot analysis were performed as described previously[43]. For solubilization of chromatin-bound histone H1, cells were suspended in a solution containing 50 mM Tris-HCl (pH 7.5), 0.5% Triton X-100, 300 mM NaCl, 60 mM $MgCl_2$, 10 mM $CaCl_2$ and DNase I (167 U ml^{-1}, Roche) and then incubated at 30 °C for 50 min.

Induction of apoptosis. Cells were incubated with etoposide (50 μM; Sigma) for 24 h, with cycloheximide (100 μg ml^{-1}; Wako) for 24 h, with staurosporine (1 μM; Sigma) for 5 h or with doxorubicin (0.5 μM or the indicated concentrations; Sigma) for 24 h. Cells were exposed to UV radiation (50 J/m^2) with an ultraviolet crosslinker UVC500 (Hoefer) and examined after 12 h.

RNAi. The retroviral vector for expression of shRNAs was described previously[43]. The hairpin sequences specific for human or mouse *CHD8* (*$CHD8_{S+L}$-1*, *$CHD8_{S+L}$-2*, *$CHD8_L$-1*, *$CHD8_L$-2*), for human *p53*, for human *histone H1A* (also effective for *H1B*, *H1C*, *H1D* and *H1E*, given the high similarity of the target region) and for enhanced green fluorescent protein (*EGFP*, Clontech) mRNAs corresponded to nucleotides 138–158 (*$CHD8_{S+L}$-1*), 814–834 (*$CHD8_{S+L}$-2*), 3808–3828 (*$CHD8_L$-1*), 4413–4433 (*$CHD8_L$-2*), 775–793 (*p53*), 262–282 (*histone H1A*) and 126–146 (*EGFP*) of the respective coding regions. The resulting vectors were used to transfect Plat E cells and thereby to generate recombinant retroviruses.

Protein identification by LC–MS/MS analysis. $CHD8_S$-associated proteins were digested with *Achromobacter* protease I and the resulting peptides were analysed with a nanoscale liquid chromatography–tandem mass spectrometry (LC–MS/MS) system as described previously[44].

Reverse transcription–polymerase chain reaction (RT–PCR) and luciferase assays. RT–PCR analysis and luciferase assays were performed as described previously[45]. Purification of mRNA from cultured blastocysts was performed with a TurboCapture mRNA kit (Qiagen). The primer sequences for RT–PCR are listed in Supplementary Information, Table S3. For luciferase assays, SaOS2 cells were transfected using FuGENE6 with expression vectors encoding human p53 or Flag-tagged wild-type or mutant versions of mouse $CHD8_S$ together with pRLTk (Promega) as an internal control and *luciferase* reporter plasmids containing promoter sequences of *PG13* or human *p21* (wild-type or mutant) genes. The cells were collected 24 h after transfection, lysed and assayed for luciferase activity with a dual-luciferase reporter assay system (Promega).

ChIP. ChIP assays were performed with a ChIP assay kit (Upstate Biotechnology) and 10^6 cells for each reaction. Precipitated DNA was quantified by real-time PCR as described previously[45]. The primer sequences are listed in Supplementary Information, Table S3.

Generation of *$Chd8^{-/-}p53^{-/-}$* mice, histopathology and culture of pre-implantation embryos. *$Chd8^{+/-}$* mice generated in our laboratory[22] were crossed with *$p53^{-/-}$* mice (Taconic Biotechnology). All mice used in this study were backcrossed to the C57BL/6 background for more than six generations. Histopathological analysis, TUNEL assay, immunohistochemistry and culture of pre-implantation embryos were performed as described previously[22]. The primer sequences for genotyping of embryos by nested PCR are listed in Supplementary Information, Table S3. All animal experiments were performed in accordance with institutional guidelines.

Note: Supplementary Information is available on the Nature Cell Biology website.

ACKNOWLEDGEMENTS

We thank T. Kitamura for pMX-puro; J. M. Cunningham and K. Hanada for the mCAT-1 plasmid; S. Miyake for the *PG13-*, *p21-*, and *p21* mutant–Luc plasmids; T. Takemori for the *NF-κB* Luc plasmid; F. Ishikawa and R. Funayama for the N-fusion and C-fusion plasmids; M. Kitagawa for HCT116 and SaOS2 cells; M. Sato, Y. Yamada, T. Moroishi, Y. Katayama, N. Nishimura and K. Oyamada for technical assistance; M. Kimura and A. Ohta for help with preparation of the manuscript; and T. Ushijima, K. Hayashi and members of the authors' laboratories for discussion. K.I.N. was supported by Takeda Science Foundation. Y.F. and A.I.S. were supported by NIH grant CA79057. Y.F. is a GCC Cancer Scholar supported by Georgia Cancer Coalition.

AUTHOR CONTRIBUTIONS

M.N. performed and planned all experiments, except some of ChIP and co-immunoprecipitation experiments, which were performed by K.O., Y.T. and T. Nakagawa; K.I.N. coordinated the study, oversaw the results and wrote the manuscript; S.I. and T. Natsume contributed to proteomic analysis; Y.F. and A.I.S. provided histone H1 triple-knockout cells and many suggestions; A.K. provided antibodies to CHD8. All authors discussed the results and commented on the manuscript.

COMPETING FINANCIAL INTERESTS

The authors declare no competing financial interests.

Published online at http://www.nature.com/naturecellbiology/
Reprints and permissions information is available online at http://npg.nature.com/reprintsandpermissions/

1. Vousden, K. H. & Lu, X. Live or let die: the cell's response to p53. *Nature Rev. Cancer* **2,** 594–604 (2002).
2. Harris, S. L. & Levine, A. J. The p53 pathway: positive and negative feedback loops. *Oncogene* **24,** 2899–2908 (2005).
3. Vogelstein, B., Lane, D. & Levine, A. J. Surfing the p53 network. *Nature* **408,** 307–310 (2000).
4. Laptenko, O. & Prives, C. Transcriptional regulation by p53: one protein, many possibilities. *Cell Death Differ.* **13,** 951–961 (2006).
5. Aylon, Y. & Oren, M. Living with p53, dying of p53. *Cell* **130,** 597–600 (2007).
6. Toledo, F. & Wahl, G. M. Regulating the p53 pathway: *in vitro* hypotheses, *in vivo* veritas. *Nature Rev. Cancer* **6,** 909–923 (2006).
7. Lavin, M. F. & Gueven, N. The complexity of p53 stabilization and activation. *Cell Death Differ.* **13,** 941–950 (2006).
8. Zhang, Y. & Xiong, Y. A p53 amino-terminal nuclear export signal inhibited by DNA damage-induced phosphorylation. *Science* **292,** 1910–1915 (2001).
9. Tanaka, T., Ohkubo, S., Tatsuno, I. & Prives, C. hCAS/CSE1L associates with chromatin and regulates expression of select p53 target genes. *Cell* **130,** 638–650 (2007).
10. Das, S. *et al.* Hzf Determines cell survival upon genotoxic stress by modulating p53 transactivation. *Cell* **130,** 624–637 (2007).
11. Lee, D. *et al.* SWI/SNF complex interacts with tumor suppressor p53 and is necessary for the activation of p53-mediated transcription. *J. Biol. Chem.* **277,** 22330–22337 (2002).
12. Kim, K. *et al.* Isolation and characterization of a novel H1.2 complex that acts as a repressor of p53-mediated transcription. *J. Biol. Chem.* **283,** 9113–9126 (2008).
13. Becker, P. B. Nucleosome remodelers on track. *Nature Struct. Mol. Biol.* **12,** 732–733 (2005).
14. Marfella, C. G. & Imbalzano, A. N. The Chd family of chromatin remodelers. *Mutat. Res.* **618,** 30–40 (2007).
15. Hall, J. A. & Georgel, P. T. CHD proteins: a diverse family with strong ties. *Biochem. Cell Biol.* **85,** 463–476 (2007).
16. Pray-Grant, M. G., Daniel, J. A., Schieltz, D., Yates, J. R., 3rd & Grant, P. A. Chd1 chromodomain links histone H3 methylation with SAGA- and SLIK-dependent acetylation. *Nature* **433,** 434–438 (2005).
17. Zhang, L., Schroeder, S., Fong, N. & Bentley, D. L. Altered nucleosome occupancy and histone H3K4 methylation in response to 'transcriptional stress'. *EMBO J.* **24,** 2379–2390 (2005).
18. Flanagan, J. F. *et al.* Double chromodomains cooperate to recognize the methylated histone H3 tail. *Nature* **438,** 1181–1185 (2005).
19. Lusser, A., Urwin, D. L. & Kadonaga, J. T. Distinct activities of CHD1 and ACF in ATP-dependent chromatin assembly. *Nature Struct. Mol. Biol.* **12,** 160–166 (2005).

20. Sakamoto, I. *et al.* A novel β-catenin-binding protein inhibits β-catenin-dependent Tcf activation and axis formation. *J. Biol. Chem.* **275,** 32871–32878 (2000).
21. Ishihara, K., Oshimura, M. & Nakao, M. CTCF-dependent chromatin insulator is linked to epigenetic remodeling. *Mol. Cell* **23,** 733–742 (2006).
22. Nishiyama, M. *et al.* Early embryonic death in mice lacking the β-catenin-binding protein Duplin. *Mol. Cell. Biol.* **24,** 8386–8394 (2004).
23. Fan, Y. *et al.* Histone H1 depletion in mammals alters global chromatin structure but causes specific changes in gene regulation. *Cell* **123,** 1199–1212 (2005).
24. Funayama, R., Saito, M., Tanobe, H. & Ishikawa, F. Loss of linker histone H1 in cellular senescence. *J. Cell Biol.* **175,** 869–880 (2006).
25. Vignali, M. & Workman, J. L. Location and function of linker histones. *Nature Struct. Biol.* **5,** 1025–1028 (1998).
26. Thomas, J. O. Histone H1: location and role. *Curr. Opin. Cell Biol.* **11,** 312–317 (1999).
27. Lusser, A. & Kadonaga, J. T. Strategies for the reconstitution of chromatin. *Nature Methods* **1,** 19–26 (2004).
28. Thoma, F., Koller, T. & Klug, A. Involvement of histone H1 in the organization of the nucleosome and of the salt-dependent superstructures of chromatin. *J. Cell Biol.* **83,** 403–427 (1979).
29. Bednar, J. *et al.* Nucleosomes, linker DNA, and linker histone form a unique structural motif that directs the higher-order folding and compaction of chromatin. *Proc. Natl Acad. Sci. USA* **95,** 14173–14178 (1998).
30. Pennings, S., Meersseman, G. & Bradbury, E. M. Linker histones H1 and H5 prevent the mobility of positioned nucleosomes. *Proc. Natl Acad. Sci. USA* **91,** 10275–10279 (1994).
31. Shimamura, A., Sapp, M., Rodriguez-Campos, A. & Worcel, A. Histone H1 represses transcription from minichromosomes assembled *in vitro*. *Mol. Cell. Biol.* **9,** 5573–5584 (1989).
32. Laybourn, P. J. & Kadonaga, J. T. Role of nucleosomal cores and histone H1 in regulation of transcription by RNA polymerase II. *Science* **254,** 238–245 (1991).
33. Shen, X., Yu, L., Weir, J. W. & Gorovsky, M. A. Linker histones are not essential and affect chromatin condensation *in vivo*. *Cell* **82,** 47–56 (1995).
34. Ushinsky, S. C. *et al.* Histone H1 in *Saccharomyces cerevisiae*. *Yeast* **13,** 151–161 (1997).
35. Patterton, H. G., Landel, C. C., Landsman, D., Peterson, C. L. & Simpson, R. T. The biochemical and phenotypic characterization of Hho1p, the putative linker histone H1 of *Saccharomyces cerevisiae*. *J. Biol. Chem.* **273,** 7268–7276 (1998).
36. Ramon, A., Muro-Pastor, M. I., Scazzocchio, C. & Gonzalez, R. Deletion of the unique gene encoding a typical histone H1 has no apparent phenotype in *Aspergillus nidulans*. *Mol. Microbiol.* **35,** 223–233 (2000).
37. Rupp, R. A. & Becker, P. B. Gene regulation by histone H1: new links to DNA methylation. *Cell* **123,** 1178–1179 (2005).
38. Wang, S. & El-Deiry, W. S. p73 or p53 directly regulates human p53 transcription to maintain cell cycle checkpoints. *Cancer Res.* **66,** 6982–6989 (2006).
39. Takagi, M., Absalon, M. J., McLure, K. G. & Kastan, M. B. Regulation of p53 translation and induction after DNA damage by ribosomal protein L26 and nucleolin. *Cell* **123,** 49–63 (2005).
40. Zahir, F. *et al.* Novel deletions of 14q11.2 associated with developmental delay, cognitive impairment and similar minor anomalies in three children. *J. Med. Genet.* **44,** 556–561 (2007).
41. Nakayama, K. *et al.* Mice lacking $p27^{Kip1}$ display increased body size, multiple organ hyperplasia, retinal dysplasia, and pituitary tumors. *Cell* **85,** 707–720 (1996).
42. Nakayama, K. *et al.* Targeted disruption of *Skp2* results in accumulation of cyclin E and $p27^{Kip1}$, polyploidy and centrosome overduplication. *EMBO J.* **19,** 2069–2081 (2000).
43. Kamura, T. *et al.* VHL-box and SOCS-box domains determine binding specificity for Cul2-Rbx1 and Cul5-Rbx2 modules of ubiquitin ligases. *Genes Dev.* **18,** 3055–3065 (2004).
44. Natsume, T. *et al.* A direct nanoflow liquid chromatography-tandem mass spectrometry system for interaction proteomics. *Anal. Chem.* **74,** 4725–4733 (2002).
45. Yada, M. *et al.* Phosphorylation-dependent degradation of c-Myc is mediated by the F-box protein Fbw7. *EMBO J.* **23,** 2116–2125 (2004).

nature cell biology

DOI: 10.1038/ncb1831

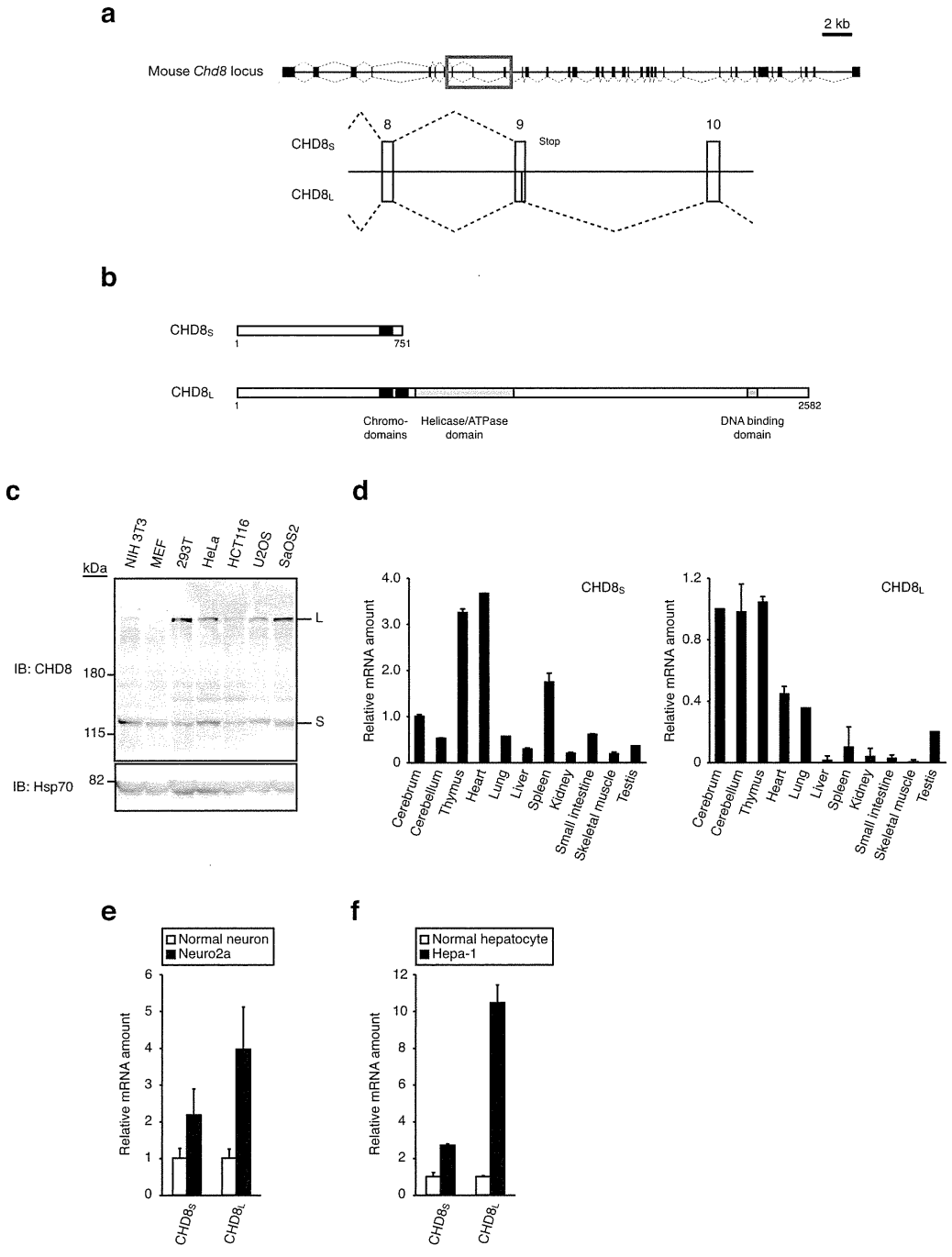

Figure S1 CHD8 has two splicing isoforms. (**a**) Organization of the mouse *Chd8* gene. The region encompassing exons 8 to 10 (red box) and containing the alternative splicing site in exon 9 is expanded in the lower scheme. (**b**) Domain structure of proteins encoded by the two alternative transcripts of *Chd8*. (**c**) Immunoblot analysis of lysates (80 μg of protein) of the indicated cell lines with anti-CHD8 and anti-Hsp70 (loading control). The positions of $CHD8_L$ (L) and $CHD8_S$ (S) are indicated. (**d**) Determination of the amounts of $CHD8_S$ and $CHD8_L$ mRNAs in mouse tissues by quantitative RT-PCR analysis. Data are expressed relative to the corresponding amount of glyceraldehyde-3-phosphate dehydrogenase (GAPDH) mRNA and are means ± SD from three independent experiments. (**e**, **f**) Expression of *Chd8* in mouse cancer cell lines and corresponding normal cells. The amounts of $CHD8_S$ and $CHD8_L$ mRNAs in Neuro2a neuroblastoma cells and normal neurons (**e**) as well as in Hepa-1 hepatoma cells and normal hepatocytes (**f**) were determined by quantitative RT-PCR analysis. Data are means ± SD from three independent experiments.

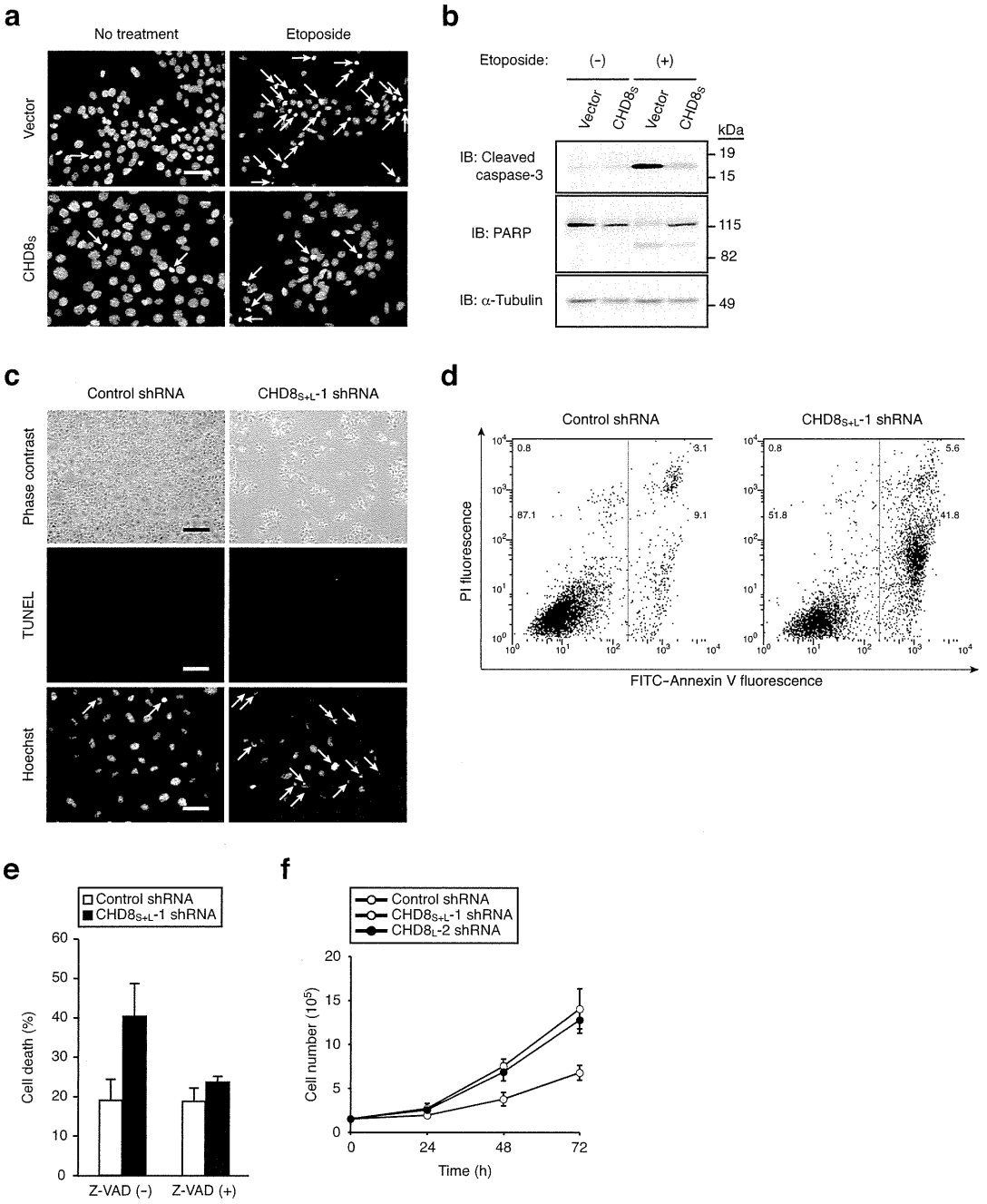

Figure S2 Inhibition of caspase-dependent apoptosis by CHD8. (**a**) NIH 3T3 cells stably infected with a retroviral vector for $CHD8_S$ or with the empty vector were exposed (or not) to etoposide and then stained with Hoechst 33258 for examination of nuclear morphology by fluorescence microscopy. Arrows indicate apoptotic cells with condensed or fragmented nuclei. Scale bar, 20 μm. (**b**) NIH 3T3 cells treated as in (**a**) were lysed and subjected to immunoblot analysis with antibodies to cleaved caspase-3, to PARP, or to α-tubulin (loading control). (**c**) HeLa cells were infected with retroviral vectors for $CHD8_{S+L}$-1 or EGFP (control) shRNAs for 96 h and then either examined by phase-contrast microscopy, subjected to the terminal deoxynucleotidyl transferase–mediated dUTP-biotin nick end-labeling (TUNEL) assay, or stained with Hoechst 33258. Arrows indicate apoptotic cells with condensed or fragmented nuclei. Scale bars, 100 μm (top panels) or 20 μm (middle and bottom panels). (**d**) HeLa cells infected as in (**c**) were stained with fluorescein isothiocyanate (FITC)–labeled Annexin V and propidium iodide (PI) and then analyzed by flow cytometry. (**e**) HeLa cells were infected with retroviral vectors for $CHD8_{S+L}$-1 or EGFP (control) shRNAs for 48 h and then incubated in the absence or presence of 50 μM Z-VAD-fmk (Peptide Institute) for 20 h. The percentage of dead cells was determined by staining with trypan blue. Data are means ± SD from three independent experiments. (**f**) HeLa cells (1.5×10^5) infected with retroviral vectors for $CHD8_{S+L}$-1, $CHD8_L$-2, or EGFP (control) shRNAs were collected after 24 h and plated in 60-mm culture dishes. Cell number was determined with a hemocytometer after the indicated times. Data are means ± SD of triplicate cultures from a representative experiment.

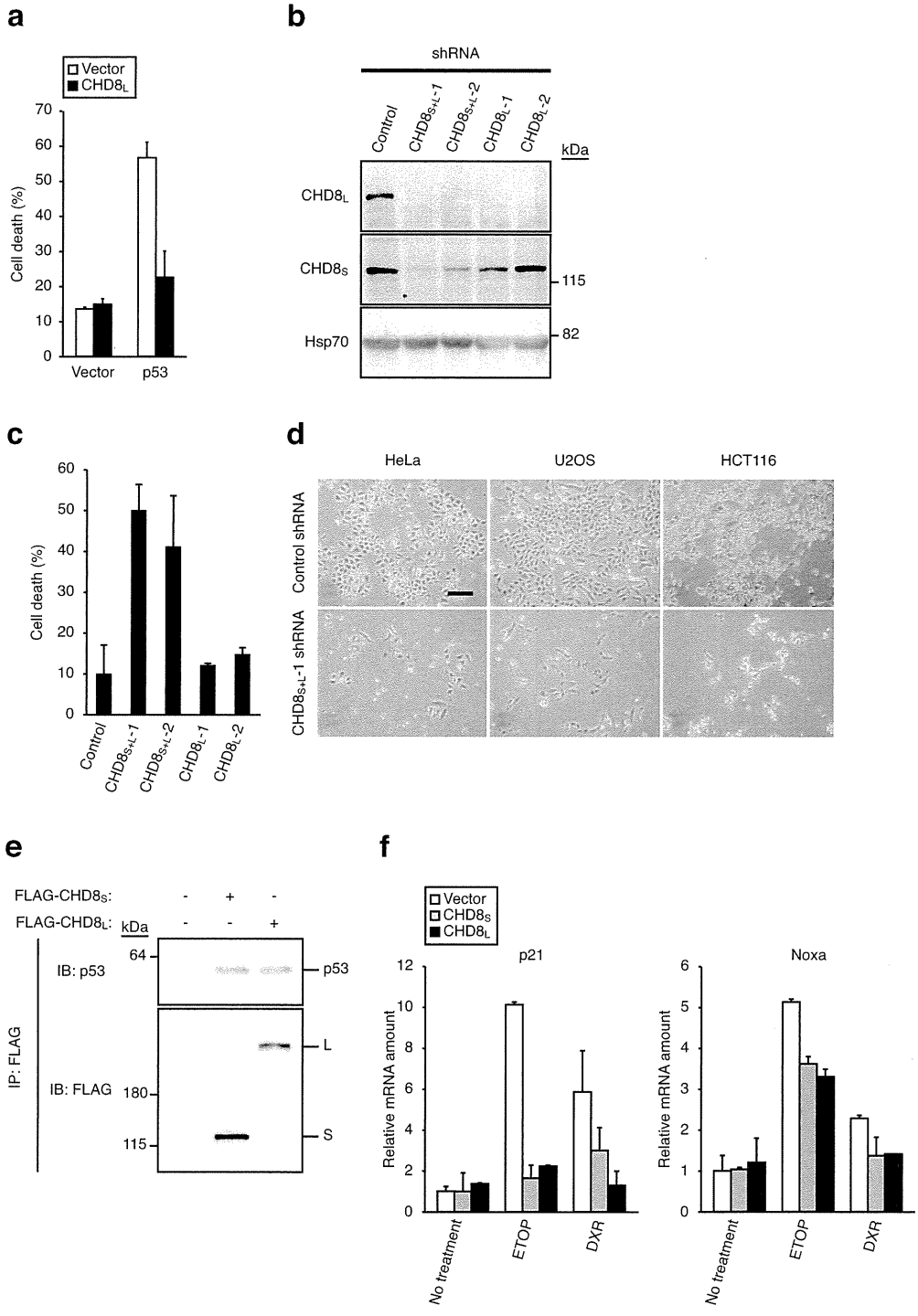

Figure S3 Both $CHD8_S$ and $CHD8_L$ inhibit p53 function. (**a**) U2OS cells were infected with retroviral vectors for $CHD8_L$ or p53 (or with the empty vector) for 72 h. The percentage of dead cells was then determined by trypan blue staining. Data are means ± SD from three independent experiments. (**b**) HeLa cells were infected with retroviral vectors encoding $CHD8_{S+L}$-1, $CHD8_{S+L}$-2, $CHD8_L$-1, $CHD8_L$-2, or EGFP (control) shRNAs. After 96 h, the cells were subjected to immunoblot analysis with anti-CHD8 or anti-Hsp70. (**c**) HeLa cells infected with retroviral vectors encoding CHD8 or EGFP (control) shRNAs were collected after 72 h and stained with trypan blue for determination of the percentage of dead cells. Data are means ± SD from three independent experiments. (**d**) HeLa, U2OS, and HCT116 cells were infected with retroviral vectors for $CHD8_{S+L}$-1 or EGFP (control) shRNAs for 72 h and then examined by phase-contrast microscopy. Scale bar, 100 μm. (**e**) HEK293T cells expressing FLAG-tagged $CHD8_S$ or $CHD8_L$ were incubated with 10 μM MG132 for 8 h and then subjected to immunoprecipitation with anti-FLAG. The resulting precipitates were subjected to immunoblot analysis with anti-p53 or anti-FLAG. (**f**) U2OS cells infected with retroviruses encoding $CHD8_S$ or $CHD8_L$ or with the empty vector were incubated in the absence or presence of etoposide (ETOP) or doxorubicin (DXR) for 24 h and then subjected to quantitative RT-PCR analysis of p21 and Noxa mRNAs. Data are means ± SD from three independent experiments.

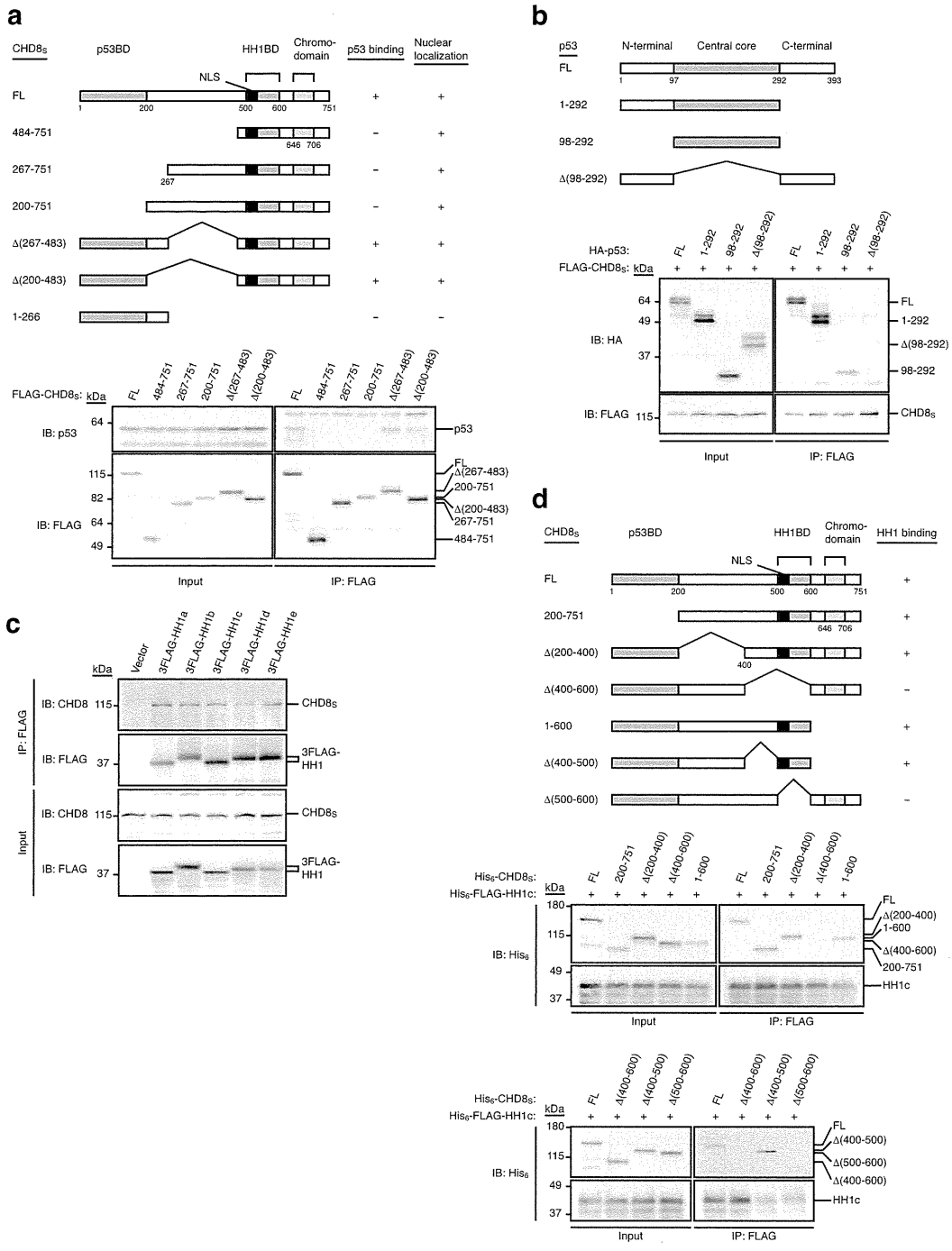

Figure S4 Molecular dissection of p53-CHD8–histone H1 interaction. (**a**) Identification of the region of $CHD8_S$ responsible for binding to p53. HEK293T cells transiently expressing the indicated FLAG-tagged $CHD8_S$ derivatives were subjected to immunoprecipitation with anti-FLAG, and the resulting precipitates (as well as 3% of the input cell lysates) were subjected to immunoblot analysis with anti-p53 or anti-FLAG (lower panel). The results for p53 binding and nuclear localization [determined by immunofluorescence analysis (data not shown)] are summarized together with schematic representations of the $CHD8_S$ derivatives tested (upper panel). p53BD, p53 binding domain; NLS, nuclear localization signal; HH1BD, histone H1 binding domain; FL, full-length. (**b**) Identification of the region of p53 responsible for binding to $CHD8_S$. HEK293T cells expressing the indicated HA-tagged p53 derivatives and FLAG-tagged $CHD8_S$ were subjected to immunoprecipitation with anti-FLAG, and the resulting precipitates (as well as 3% of the input cell lysates) were subjected to immunoblot analysis with anti-HA or anti-FLAG. (**c**) All five major variants of histone H1 interact with CHD8 in vivo. HEK293T cells expressing mouse histones H1a, H1b, H1c, H1d, or H1e tagged with three copies of the FLAG epitope, or those transfected with the empty vector, were lysed and subjected to immunoprecipitation with anti-FLAG. The resulting precipitates, as well as 3% of the original cell lysates (input), were subjected to immunoblot analysis with anti-CHD8 or anti-FLAG. (**d**) Identification of the region of $CHD8_S$ responsible for binding to histone H1. Recombinant His_6-tagged $CHD8_S$ derivatives and His_6- and FLAG-tagged histone H1c (HH1c) were mixed and subjected to immunoprecipitation with anti-FLAG, and the resulting precipitates as well as 10% of the original binding mixtures (input) were subjected to immunoblot analysis with anti-His_6 (right panels). The results of the binding assay are summarized together with schematic representations of the $CHD8_S$ derivatives (left panel).

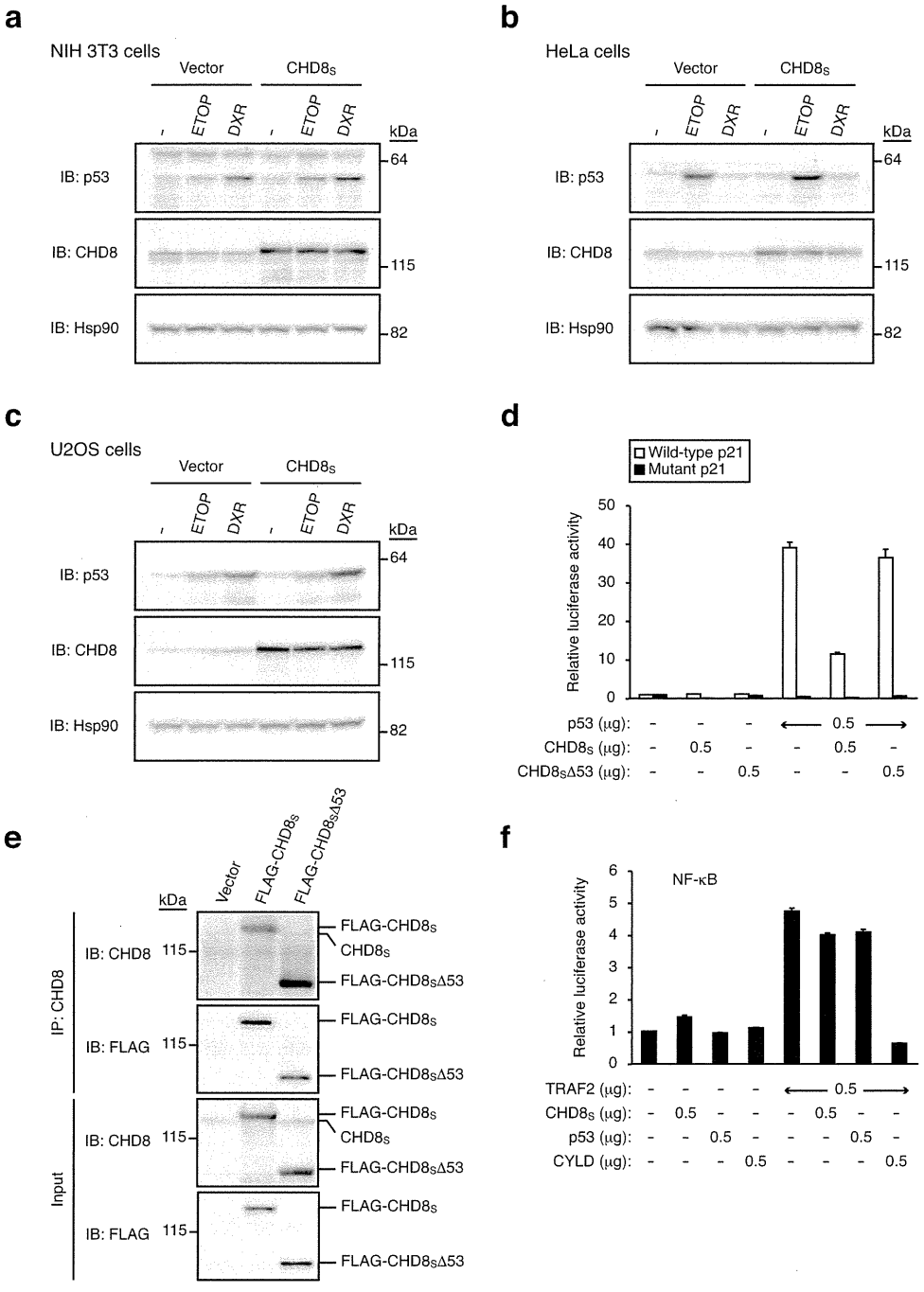

Figure S5 CHD8 is a specific inhibitor of p53-dependent transactivation. (**a**–**c**) Abundance of p53 and CHD8 in cells overexpressing CHD8 and subjected to genotoxic stress. NIH 3T3 (**a**), HeLa (**b**), or U2OS (**c**) cells infected with a retrovirus for $CHD8_S$ or with the empty vector were incubated in the absence (–) or presence of etoposide (ETOP) or doxorubicin (DXR) for 24 h. The cells were then subjected to immunoblot analysis with anti-p53, anti-CHD8, or anti-Hsp90. (**d**) SaOS2 cells were transfected with the indicated amounts of expression vectors for p53 and either wild-type or mutant (Δ53) $CHD8_S$ together with a luciferase reporter plasmid containing wild-type or mutant forms of the *p21* promoter, the latter of which harbored mutations in p53RE1 and p53RE2. The cells were then incubated for 24 h before assay of relative luciferase activity. Data are means ± SD of triplicates from a representative experiment. (**e**) HEK293T cells transiently expressing FLAG-tagged wild-type or mutant (Δ53) $CHD8_S$ were subjected to immunoprecipitation with anti-CHD8. The resulting precipitates, as well as 3% of the original cell lysates (input), were subjected to immunoblot analysis with anti-CHD8 or anti-FLAG. (**f**) HEK293T cells were transfected with the indicated amounts of expression vectors for TRAF2, $CHD8_S$, p53, and CYLD together with a luciferase reporter plasmid containing three binding sites for NF-κB. The cells were then incubated for 24 h before assay of relative luciferase activity. TRAF2 expression increased the luciferase activity derived from this construct, but this effect of TRAF2 was not inhibited by overexpression of $CHD8_S$ or p53. In contrast, CYLD, a deubiquitinating enzyme that is a negative regulator of the NF-κB signaling pathway, markedly inhibited the TRAF2 effect. Data are means ± SD of triplicates from a representative experiment.

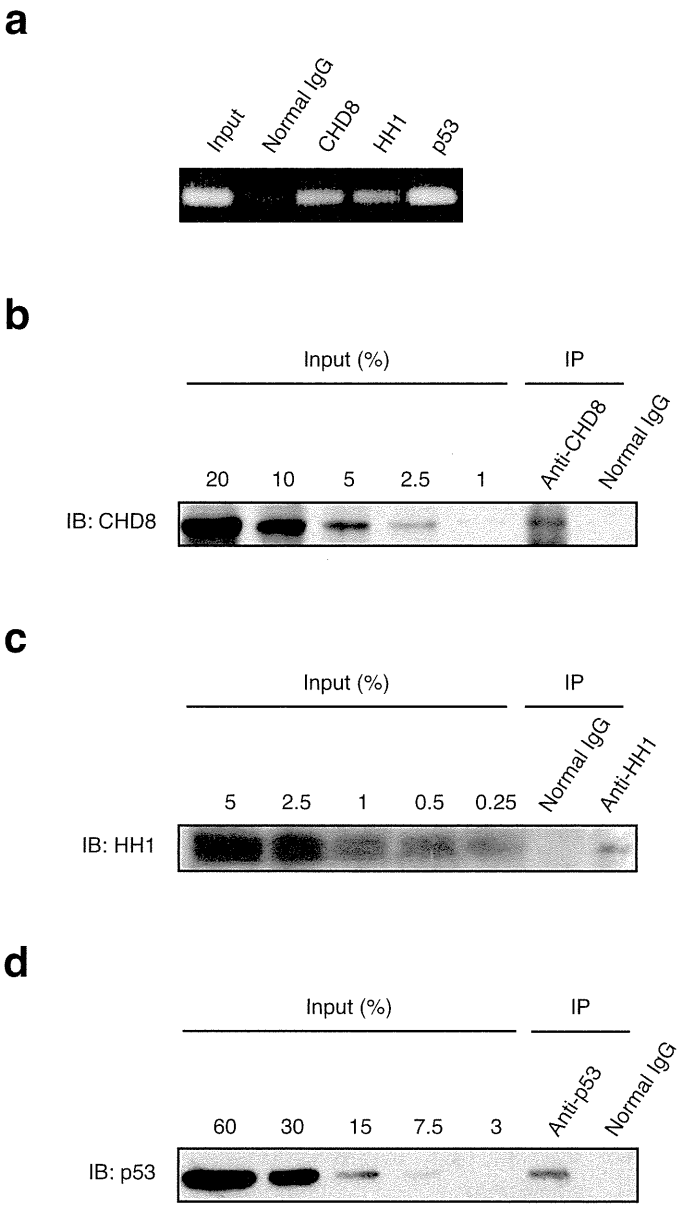

Figure S6 Antibody specificity and immunoprecipitation efficiency for ChIP. (**a**) U2OS cells infected with a retroviral vector encoding $CHD8_S$ were incubated with etoposide for 24 h, lysed, and subjected to ChIP with anti-CHD8, anti–histone H1, or anti-p53 or with control IgG. The precipitated DNA (as well as 1% of the input cell lysates) was subjected to PCR analysis with primers specific for p53RE1 of the *p21* promoter. (**b–d**) U2OS cells treated as in (**a**) were subjected to ChIP with anti-CHD8 (**b**), anti–histone H1 (**c**), or anti-p53 (**d**). The resulting precipitates as well as the indicated percentages of the original cell lysates (input) were subjected to immunoblot analysis with the corresponding antibodies. By comparing the amounts of input and immunoprecipitated proteins, we determined the ChIP efficiency to be ~5% for CHD8 (**b**), 0.1% for histone H1 (**c**), and 15% for p53 (**d**).

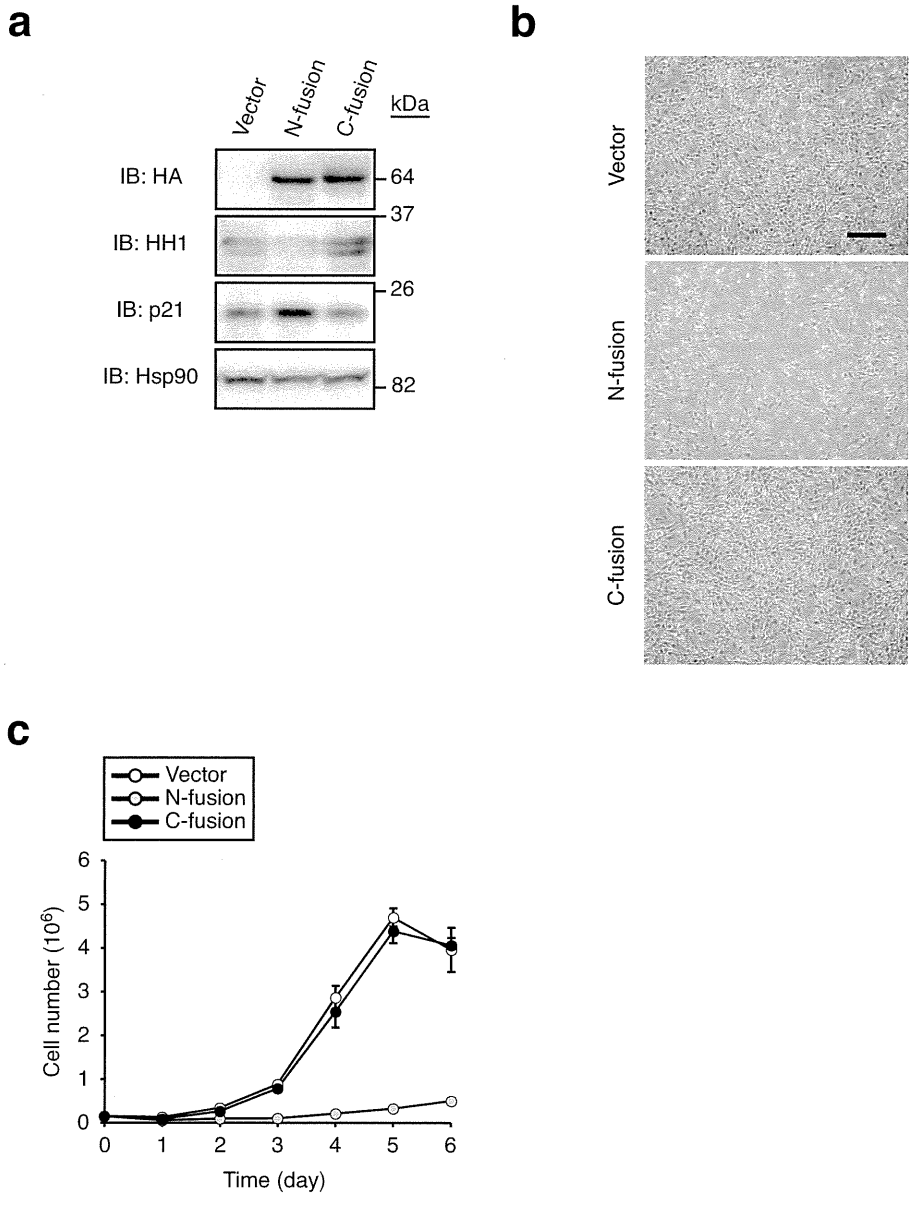

Figure S7 Effects of expression of histone H1 mutants. (**a**) NIH 3T3 cells were infected with retroviral vectors encoding histone H1 tagged at its NH_2-terminus (N-fusion) or COOH-terminus (C-fusion) with EGFP (or with the empty vector) for 96 h and were then subjected to immunoblot analysis with anti-HA (both fusion proteins were also tagged at their NH_2-termini with HA), anti–histone H1, anti-p21, or anti-Hsp90 (loading control). (**b**) NIH 3T3 cells infected as in (**a**) were examined by phase-contrast microscopy. Scale bar, 100 μm. (**c**) NIH 3T3 cells (1.5×10^5) infected as in (**a**) were collected after 24 h and plated in 60-mm culture dishes. Cell number was determined with a hemocytometer after the indicated times. Data are means ± SD of triplicate cultures from a representative experiment.

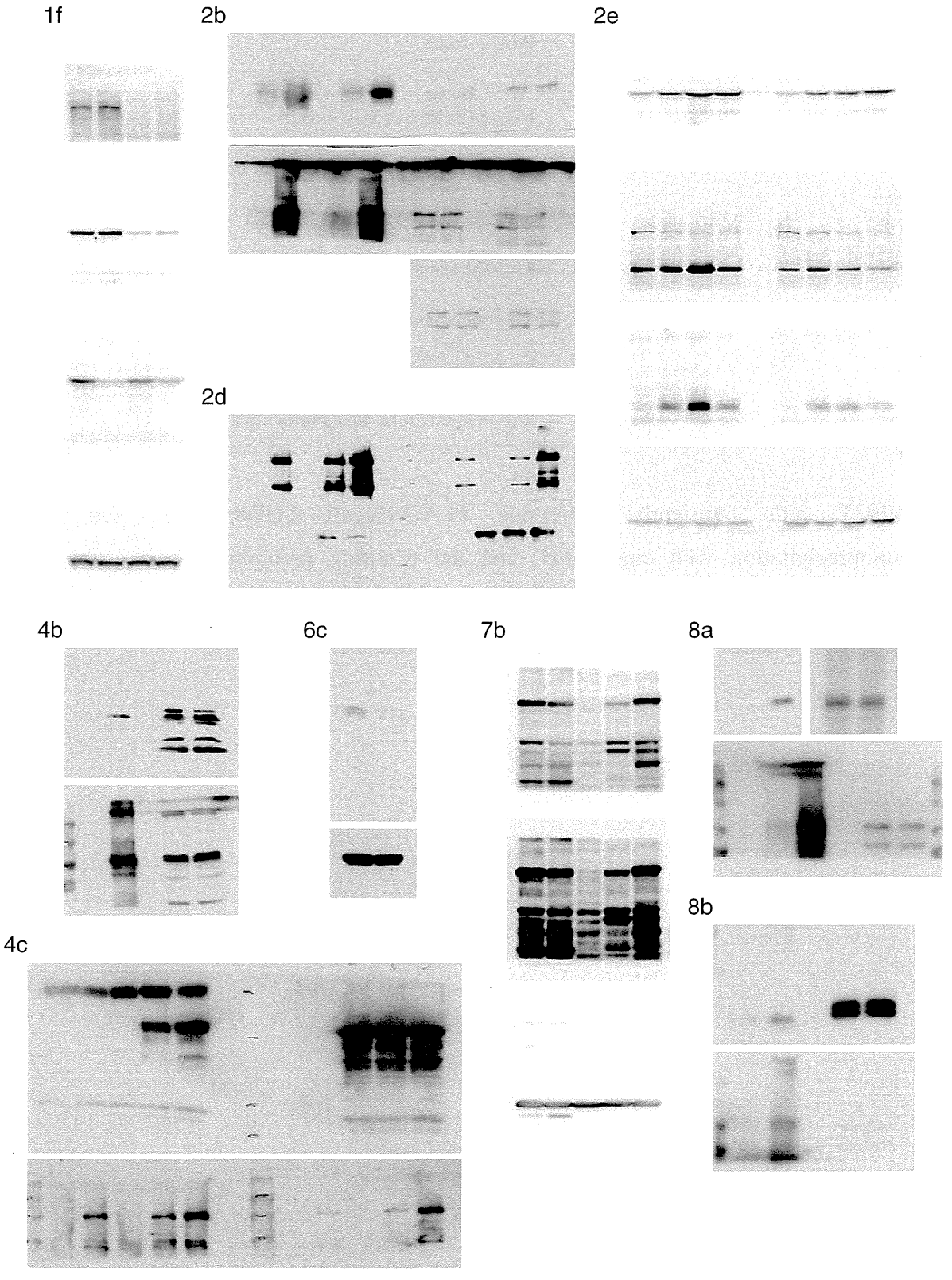

Figure S8 Full scans of key immunoblots in the indicated figures.

Table S1. Identification of CHD8-associated proteins by proteomics analysis.

Gene symbol	Protein name	Sequence coverage (%)
HIST1H1E/HIST1H1C/HIST1H1D	Histone 1; H1e or H1c or H1d	23.5
KPNA2	Karyopherin alpha 2 (RAG cohort 1, importin alpha 1)	22.3
KPNA1	Karyopherin alpha 1 (importin alpha 5)	18.2
KPNA3	Karyopherin alpha 3 (importin alpha 4)	16.6
KPNB1	Karyopherin (importin) beta 1	14.4
KPNA4	Karyopherin alpha 4 (importin alpha 3)	11.7

HEK293T cells transiently expressing FLAG-tagged $CHD8_S$ were subjected to immunoprecipitation with anti-FLAG, and the resulting precipitates were subjected to LC–MS/MS analysis. Proteins reproducibly detected in four independent experiments are listed. The percentage sequence coverage for each protein is also shown.

Table S2. Genotype of embryos from *Chd8*$^{+/-}$*p53*$^{+/-}$ mouse intercrosses.

E7.5	*p53*$^{+/+}$	*p53*$^{+/-}$	*p53*$^{-/-}$	Total
Chd8$^{+/+}$	4	9	3	16
Chd8$^{+/-}$	7	14	5	26
Chd8$^{-/-}$	2	5	3	10
Total	13	28	11	52

E8.5	*p53*$^{+/+}$	*p53*$^{+/-}$	*p53*$^{-/-}$	Total
Chd8$^{+/+}$	2	7	3	12
Chd8$^{+/-}$	9	26	11	46
Chd8$^{-/-}$	1	5	3	9
Total	12	38	17	67

E9.5	*p53*$^{+/+}$	*p53*$^{+/-}$	*p53*$^{-/-}$	Total
Chd8$^{+/+}$	5	16	8	29
Chd8$^{+/-}$	10	36	10	56
Chd8$^{-/-}$	0	4	8	12
Total	15	56	26	97

Embryos from *Chd8*$^{+/-}$*p53*$^{+/-}$ mouse intercrosses were dissected from uteri between E7.5 and E9.5 and genotyped by PCR.

Table S3. Primer sequences (5′→3′) for nested PCR, RT-PCR, and ChIP analyses.

Gene (primer)	Forward primer	Reverse primer
	Nested PCR	
mp53 (Mutant-1st)	GTGTTCCGGCTGTCAGCGCA	AGCGTCTCACGACCTCCGTC
mp53 (Wild type-1st)	ACACACCTGTAGCTCCAGCAC	AGCGTCTCACGACCTCCGTC
mp53 (Mutant-2nd)	CCCGGTTCTTTTTGTCAAGAC	ATGTGCTGTGACTTCTTGTAG
mp53 (Wild type-2nd)	TGGGGAGGCCAAAGTGGGAGG	ATGTGCTGTGACTTCTTGTAG
mChd8 (Mutant-1st)	TGCTAAAGCGCATGCTCCAGACTG	AACTCCGTAACCATTTGTCTATTC
mChd8 (Wild type-1st)	TATAGATTTCCTGTTTGATTTTCC	AACTCCGTAACCATTTGTCTATTC
mChd8 (Mutant-2nd)	ATGCTCCAGACTGCCTTGGGAAAA	GAAACAATGTAAAACAGGCAAATG
mChd8 (Wild type-2nd)	AAAGAATCACACTAGATCTAATCC	GAAACAATGTAAAACAGGCAAATG
	RT-PCR	
$mChd8_S$	CAGATGAGACACTTCTTTCATGAA	TTCTCCGCGCCCAACTCAC
$mChd8_L$	CAGATGAGACACTTCTTTCATGAA	TTTTACCAGGTAGTAAATTACAGG
mp21	TGTCTTGCACTCTGGTGTCTGAGC	TCTTGCAGAAGACCAATCTGCG
hp21	CTGAGACTCTCAGGGTCGAA	CGGCGTTTGGAGTGGTAGAA
mNoxa	ACTCAGGAAGATCGGAGACAAAGTG	ACACTCGTCCTTCAAGTCTGCTGG
hNOXA	AGAGCTGGAAGTCGAGTGT	GCACCTTCACATTCCTCTC
mGapdh	GCCTGGAGAAACCTGCCAAGTATG	GAGTGGGAGTTGCTGTTGAAGTCG
hGAPDH	GCAAATTCCATGGCACCGT	TCGCCCCACTTGATTTTGG
	ChIP	
hp21 (p53RE1)	CAGGCTGTGGCTCTGATTGG	TTCAGAGTAACAGGCTAAGG
hp21 (p53RE2)	GGTCTGCTACTGTGTCCTCC	CATCTGAACAGAAATCCCAC
hp21 (CR)	GGTGCTTCTGGGAGAGGTGAC	TGACCCACTCTGGCAGGCAAG
hBAX (p53RE)	TTGGAAGGCTGAGACGGGGTTATC	AGAAGTTTCGGGCAGGGTTTGAG
hBAX (CR)	CCTGCTGATCTATCAGCACAG	GCTGGTCTCTGAACTCCCAGA
hp27	CCGCCGCCGCAACCAATGGAT	GGAGTCGCAGAGCCGTGAGCA

Mouse and human genes are indicated by m and h, respectively.

The Prostate 72:626–637 (2012)

Identification of Phosphorylated Proteins Involved in the Oncogenesis of Prostate Cancer Via Pin1-Proteomic Analysis

Kanji Endoh,[1,2] Mayuko Nishi,[2] Hitoshi Ishiguro,[3,4] Hiroji Uemura,[3] Yohei Miyagi,[5] Ichiro Aoki,[6] Hisashi Hirano,[7] Yoshinobu Kubota,[3] and Akihide Ryo[2]*

[1]Drug Discovery Research Center, Taiho Pharmaceutical Co., Ltd, Tsukuba, Japan
[2]Department of Microbiology, Yokohama City University School of Medicine, Yokohama, Japan
[3]Department of Urology, Yokohama City University School of Medicine, Yokohama, Japan
[4]Photocatalyst Group, Kanagawa Academy of Science and Technology, Takatsu-ku, Kawasaki, Kanagawa, Japan
[5]Molecular Pathology and Genetics Division, Kanagawa Cancer Center Research institute, Yokohama, Japan
[6]Department of Molecular Pathology, Yokohama City University School of Medicine, Yokohama, Japan
[7]Department of Nanobioscience, Yokohama City University, Yokohama, Japan

BACKGROUND. The peptidyl-prolyl isomerase Pin1 regulates a subset of phosphorylated proteins by catalyzing the *cis-trans* isomerization of their specific phosphorylated Ser/Thr-Pro motifs. Although Pin1 has been shown to be involved in cell transformation and the maintenance of the malignant phenotype in prostate cancer, its specific substrates during these processes have not yet been determined.

METHODS. Cancer-specific phosphorylated proteins were isolated from two human prostate cancer cell lines (PC-3, LNCaP) and the Dunning rat prostate cancer cell lines by GST-pull down analysis with recombinant GST-Pin1 protein. These proteins were then identified by the LC-MS/MS analysis using a Q-Tof micro mass spectrometer and processed for further functional analysis.

RESULTS. We newly identified five prostate cancer-specific Pin1 binding proteins (PINBPs) in this screen. Among these, TRK-fused gene (TFG) was found to be preferentially up-regulated in prostate cancer cell lines and tissues. The targeted inhibition of TFG by specific siRNA resulted in the reduced cell proliferation and the induction of premature senescence in PC3 prostate cancer cells. We further found that TFG can facilitate the cell signaling mediated by NF-kappaB and androgen receptor (AR). Tissue micro-dissection based quantitative RT-PCR analysis of prostate cancer tissues following radical prostatectomy further revealed that TFG expression is closely associated with both a higher probability and shorter period of tumor recurrence following surgery.

CONCLUSIONS. Pin1-based proteomics analysis is a useful tool for the identification of prostate cancer-specific phosphorylated proteins. TFG could be a potential diagnostic and/or prognostic marker and therapeutic target in prostate cancer. *Prostate 72:626–637, 2012.* © 2011 Wiley Periodicals, Inc.

KEY WORDS: **prostate cancer; tumor recurrence; androgen receptor; prognostic marker**

INTRODUCTION

Prostate cancer is one of the most common tumors to arise in males and its incidence is increasing steadily worldwide [1]. Despite the possibility of an earlier diagnosis using serum prostate specific antigen (PSA), prostate cancer is still the leading cause of male cancer death in many countries [2]. Radiation and a radical prostatectomy are definitive forms of therapy for clinically localized prostate cancers, but a

Grant sponsor: Special Coordination Funds for Promoting Science and Technology; Grant sponsor: Takeda Foundation; Grant sponsor: Uehara Memorial Foundation; Grant sponsor: Grant-in-Aid for Scientific Research on Innovative Areas.

*Correspondence to: Prof. Akihide Ryo, PhD, MD, Yokohama City University School of Medicine, 3-9 Fukuura, Kanazawa-ku, Yokohama 236-0004, Japan. E-mail: aryo@yokohama-cu.ac.jp

Received 21 March 2011; Accepted 1 July 2011
DOI 10.1002/pros.21466
Published online 1 August 2011 in Wiley Online Library (wileyonlinelibrary.com).

substantial number of cases have demonstrated tumor recurrence, even when tumors have been localized pathologically to the prostate at the time of surgery. Recurrent cancers after radiation and radical prostatectomy are often refractory to treatments with chemical reagents and radiation [3,4]. Although the Gleason grade is an excellent diagnostic indicator of prostate cancer based on histopathological features, it is currently difficult to predict whether a clinically localized prostate cancer will remain latent or progress to aggressive or metastatic disease [5]. Novel prostate cancer biomarkers based on the molecular cell biology of prostate tumorigenesis are thus desirable.

Recent advances in mass spectrometry (MS) have enabled the analysis of not only overall protein expression profiling in certain cancer cells or tissues [6–8], but also a substantial number of post-translational modifications (PTMs), such as protein phosphorylation, from small cancer tissue specimens in a short timeframe. Whilst these technically advanced MS methods can detect a large number of candidate proteins [9,10], it remains difficult to select functionally significant oncoproteins and the corresponding PTMs that contribute to the progression of cellular oncogenesis. It is thus desirable to develop a new strategy for selectively capturing phosphorylated proteins that are functionally important in cell transformation and oncogenesis.

Pin1 is an enzyme that specifically binds phosphorylated serine or threonine, immediately preceding proline (pSer/Thr-Pro) in a subset of proteins [11]. Pin1 regulates the function of its substrate proteins by promoting *cis/trans* isomerization of the peptide bond between Ser/Thr and Pro [12,13]. We previously demonstrated that the peptidyl prolyl-isomerase Pin1 plays an important role in the maintenance of the tumorigenic properties of prostate cancer [14]. Targeted depletion of Pin1 results in the stable suppression of both cell growth and tumorigenicity in prostate cancer cells [14]. Furthermore, Pin1 inhibition significantly suppresses several malignant phenotypes such as cell proliferation, invasion, and angiogenesis. These results indicate that Pin1 plays crucial role in a range of tumorigenic properties in prostate cancer cells. However, specific Pin1 substrates during these processes have not so far been determined.

In our present study, we utilized Pin1 as a molecular probe in combination with MS analysis to capture and identify prostate cancer-specific phosphorylated proteins. We thereby identified TRK-fused gene (TFG) as a new Pin1-interacting oncogenic protein and provide evidence that it could be a potent therapeutic target for prostate cancer.

MATERIALS AND METHODS

Cell Lines

DU145, PC3, and LNCaP cells (human prostate cancer cell lines) were obtained from the American Type Culture Collection (Rockville, MD). Prostatic epithelial cells (hPrEC) were purchased from Takara Bio (Shiga, Japan). PrEC were cultured in prostate epithelial basal medium (PrEBM, Takara Bio) supplemented with human epidermal growth factor, triiodothyronine, transferrin, epinephrine, gentamicin sulfate, amphotericin B, bovine pituitary extract, bovine insulin, hydrocortisone, and retinoic acid additives provided by the manufacturer. Prior to the experiments, DU145, LNCaP, and PC3 cells were cultured in RPMI1640 (Wako, Osaka, Japan) supplemented with 10% fetal calf serum (FCS), and incubated under 5% CO_2. In the experiments, these cells were cultured in phenol red-free RPMI plus 0.1% bovine serum albumin (BSA) or F-12 medium supplemented with charcoal-stripped 10% FCS, and stimulated with reagents.

Pin1 Proteomic Analysis

GST-fused Pin1 was purified using a conventional strategy in *E. Coli* and used in pull down analysis with cell lysates. Prostate cancer or normal prostate epithelial cell lysates were processed for pull down with GST or GST-Pin1 at 4°C for 3 hr. Pin1-binding proteins were thereby recovered and collected by thrombin cleavage which digests at a site between GST and Pin1 followed by SDS–PAGE, as described previously [15]. Gels were subjected to silver staining and specific bands were systematically excised. The gel pieces were then reduced, alkylated, and trypsinized. Peptides were analyzed by liquid chromatography-tandem MS (LC-MS/MS) analysis with a Q-Tof micro Mass Spectrometer (Micromass). Protein identification was performed using a Mascot search (Matrix Science).

RNA Extraction, cDNA Preparation, Real-Time RT-PCR, and siRNA

Total RNA was extracted using ISOGEN reagent (Nippon Gene, Tokyo, Japan). Quantitative reverse transcription (qRT)-PCR was performed with an ABI 7700 sequence detector system (Applied Biosystems) as described previously. Primers for TFG (5′-GGAACACAAAAGACCAAAATGG-3′; 5′-AGGGCTCTACTTTAGTACATC-3) were designed using Primer Express (Applied Biosystems). Reagents from the One-Step Cyber Green RT-PCR Master Mix Reagents Kit (TaKaRa) were used in accordance with the

manufacturer's protocol. PCR reactions were performed in a total volume of 25 μl using ABI Prism770 (Applied Biosystems). A standard curve method was used to determine the expression levels and all measurements were found to be within the linear range of the standard curve. β-actin was used as an internal control and to normalize Pin1 expression levels. TFG-targeted siRNA sequences were as follows: (TFG1: 5′-GUCUGCUUCUGAUUCUUCU-3′; TFG2: 5′- GGUCAGAUGUACCAACAGU -3′; control: 5′- UCGTAUGUUGUGUGGAAUU -3′).

Cell Culture

Human prostate cancer cell lines PC3, LNCaP, and DU145 were cultured in RPMI1640 or DMEM, supplemented with 10% FCS and penicillin/streptomycin. Dunning rat tumor sub lines of variable cell growth (doubling time, days) and variable degrees of metastatic potential; AT-1 (2.5 ± 0.2 days, 0–5%), AT-2 (2.5 ± 0.2 days, 0–20%), AT-3 (1.8 ± 0.2 days, 75–100%), and MAT-LyLu (1.7 ± 0.3 days, 75–100%) were grown in RPMI 1,640/10% fetal bovine serum (FBS) supplemented with 0.1% dexamethasone and 1% L-glutamine [16].

Antibodies

An anti-TFG polyclonal antibody was generated in rabbits against a synthetic peptide corresponding to the region 320–336 of TFG conjugated to keyhole limpet hemocyanin, and purified on a peptide affinity column. TFG phospho-specific polyclonal antibodies (anti-TFGpThr206 and anti-TFGpThr372) were generated in rabbits against synthetic peptides "CEDRSGpTPDSIX" and "CXXGSTMpTPPPSX" (where X donates any one of the 20 amino acids) respectively, as described previously [17]. Antibodies were affinity-purified on sepharose resin to which the appropriate phosphorylated peptide had been covalently coupled and passed through a column containing the unphosphorylated peptides to remove any antibodies that did not recognize the phosphorylated epitope. Phosphospecificity was established by ELISA and western blot assays.

Gene Reporter Assay

Cells were transfected with plasmid vectors encoding either NF-kB-Luc or PSA-Luc reporter construct and co-transfected with pRL-TK or pRL-SV40 using Effectene transfection reagent (Qiagen). One day after transfection, the cells were resuspended in passive lysis buffer (Promega) and incubated for 15 min at room temperature. Luciferase activities were measured with a Dual-Luciferase reporter assay system (Promega) according to the manufacturer's instructions.

Patients and Samples

Paired human untreated primary prostate cancer tissues and normal (or benign prostatic hypertrophy (BPH) (n = 29)) tissues from same patients were obtained during radical prostatectomy at Yokohama City University Hospital and its affiliates. The clinicopathological data for these samples are summarized in Table I. The postoperative serum PSA levels were assayed every 2–3 months. The occurrence of these consecutive elevations of the PSA level by more than 0.20 ng/ml was defined as biochemical recurrence [18]. The pathological stage was determined according to the International Union against Cancer (UICC) [19]. The sampling and usage of all prostate tissues in this study were approved by the ethical committee of Yokohama City University Graduate School of Medicine and performed only after obtaining informed consent from each patient.

Statistics

All statistical analyses were performed using a software for statistic analysis PASW statistics 18 (SPSS, Chicago, IL). TFG expressions and clinicopathological characteristics were compared using chi-square test or the Fisher's exact test. For analysis of the correlation between TFG expression, clinicopathological characteristics, and biochemical recurrence, Kaplan–Meier and log rank tests were utilized. Each parameter and biochemical recurrence was further analyzed using a Cox promotional hazard regression model in univariate and multivariate analyses. The hazard ratio and 95% confidence interval (95%) are also shown in the results. $P \leq 0.05$ was considered to be statistically significant.

TABLE I. Clinicopathological Characteristics of Examined Prostate Cancer Samples

		n	(%)
Age (years)	≦68	15	51.7
	>68	14	48.3
Median(Range)	68(52–75)		
Preoperative PSA(ng/ml)	≦10.0	15	51.7
	>10.0	14	48.3
Median(Range)	8.8(4.1–35.7)		
UICC Stage	pT2a-b	16	55.2
	pT3a-b	13	44.8
Gleason score	≦7	20	69.0
	>8	9	31.0

RESULTS

Isolation of Prostate Cancer-Specific Phosphorylated Proteins using Pin1 Proteomics

Previous reports of Pin1-prostate cancer interaction have demonstrated that Pin1 contributes to the transformation and tumorigenicity of prostate epithelial cells by modulating the function of its substrate proteins [20]. To identify prostate cancer-specific Pin1 substrates, we performed proteomics analysis in which Pin1 was used as a molecular probe to detect phosphorylated targets. We detected multiple bands in then prostate cancer cell lines that were not present in normal prostate epithelial cells. These bands were excised from the gel and subjected to in-gel digestion followed by LC-MS/MS analysis with a Micromass Q-Tof micro Mass Spectrometer. We identified five Pin1 binding proteins (PINBP 1-5) specific to prostate cancer cells (Fig. 1, left panel).

We next performed parallel experiments using the Dunning rat tumor model developed by Issacs et al. [16]. This is a well-characterized animal model that has been used to study prostate cancer pathogenesis. These cell lines have also been shown to exhibit many characteristics including the androgen responsiveness and differential metastatic ability observed during the progression of human prostate cancer. We investigated Pin1-binding proteins in several Dunning tumor sublines (AT1, AT-2, AT-3, and MAT-LyLu), the spectra of which are illustrated in Figure 1 (right panel). When we evaluated the differences in the PINBP profiles for each subline, a 55 kDa band was found to be prominent. This band intensity was significantly increased in malignant Dunning tumor cells. Subsequent LS-MS/MS analysis revealed that the corresponding protein is derived from rat TFG. Since TFG was also identified as a Pin1-interacting protein in human prostate cancer cell lines, we focused on this protein for further analysis.

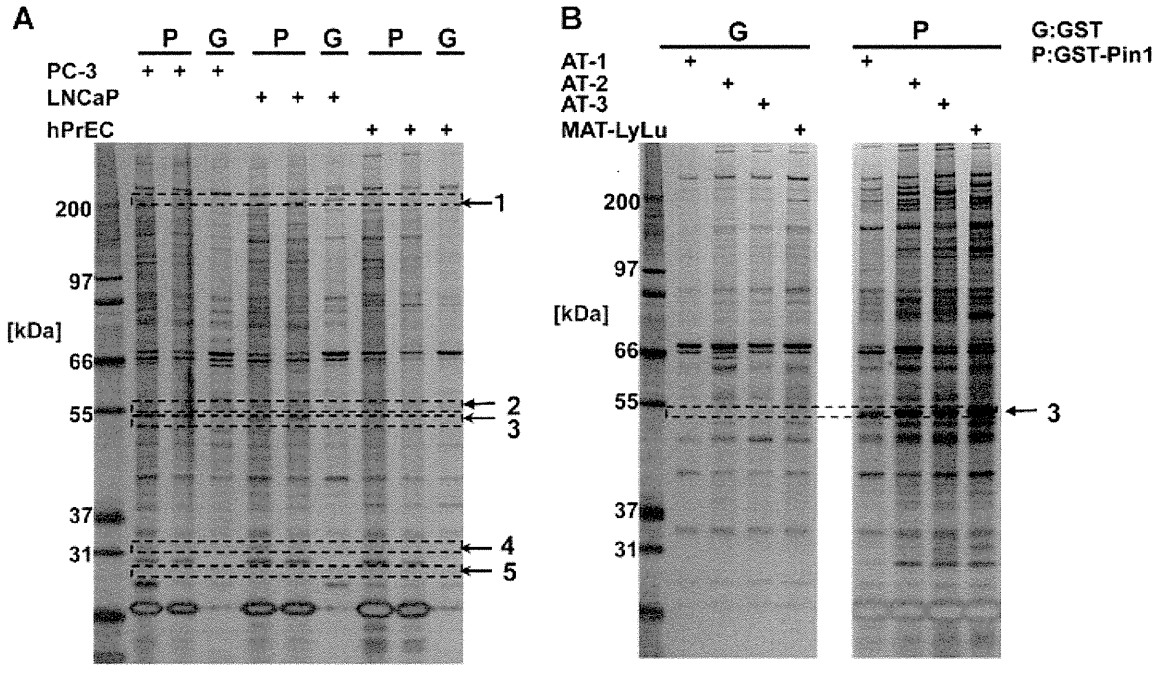

No	protein	accession No	AA
1	Microtuble-associated protein 1A	NP 002364 5	2803
2	Non-POU protein	AAH69636	471
3	TFG protein	NP_001007566	400
4	necleophosmin	AAA36380.1	294
5	Complement component 1	NPQ07021	282

Fig. 1. Identification of TFG as a Pin1 binding protein in prostate cancer cells. **A**: Cell lysates of PC-3, LNCaP, or normal prostatic epithelial cells (hPrEC) were subjected to pull down analysis with either GST or GST-Pin1. Proteins bound to glutathione sepharose beads were isolated and detected by SDS–PAGE and silver staining. Arrows point to the bands containing TFG protein. **B**: Cell lysates from each Dunning subline were processed for GST-pull down analysis as in (A). Bound proteins were separated by SDS–PAGE and detected by sliver staining. Arrow indicates the bands containing TFG protein.

TFG is Overexpressed in Prostate Cancer Cells and Tissues

Our initial analysis indicated that TFG is a Pin1-binding protein in prostate cancer cells and we thus examined its expression in these cells. Both quantitative RT-PCR analysis and immunoblotting with TFG antibodies revealed that TFG expression is preferentially up-regulated in prostate cancer cell lines as compared with normal prostate epithelial cells (Fig. 2A and B). Immunohistochemical analysis of representative prostate cancer tissues with TFG antibodies further revealed that TFG is expressed in glandular cancer cells but not in adjacent non-cancerous epithelial cells (benign prostatic hyperplasia: BPH) or interstitial cells (Fig. 2C). Since prostate cancer cells often infiltrate non-cancerous glands and the intervening fibro-muscular stroma, it was necessary to precisely quantitate the TFG expression levels in cancerous glandular cells. We utilized tissue microdissection based quantitative RT-PCR analysis for this purpose. Twenty nine paired human prostate cancer and adjacent non-cancerous prostate tissues from the same individual were thereby examined. The results of this analysis showed that the TFG expression levels in prostate cancer tissues are higher than in non-cancerous tissues in 63.9% ($P = 0.031$) of the cases (Fig. 2D). These results together demonstrate that TFG is overexpressed in prostate cancer cells.

TFG Interacts With Pin1 on its Thr206-Pro and Thr372-Pro Motifs

Previous reports have indicated that Pin1 can bind only phosphorylated Ser/Thr-Pro motifs [21] of which only two (Thr206-Pro and Thr372-Pro) are present in the TFG protein (Fig. 3A, upper). Interestingly, this motif is conserved between various species including human, rhesus monkey, mouse, and xenopus (Fig. 3A, lower). We thus generated TFG site-directed mutants at these sites by substituting threonine with alanine (T206A, T372A). GST-pull down

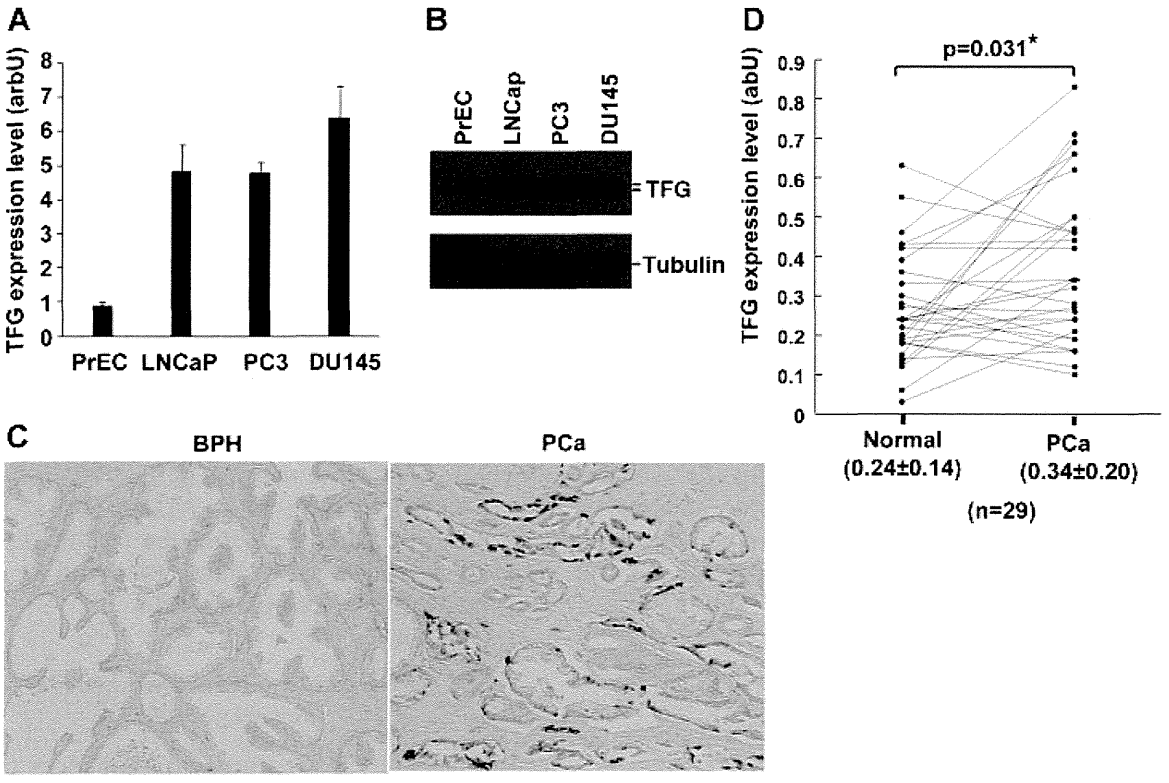

Fig. 2. TFG is overexpressed in prostate cancer cells and tissues. **A, B**: TFG mRNA expression levels were monitored by quantitative RT-PCR analysis of normal prostatic epithelial cells (PrEC) or three different prostate cancer cell lines (A). Cell lysates from the indicated cells were subjected to immunoblot analysis with either anti-TFG or anti-tubulin antibody. Tubulin was used as a loading control. **C**: Immunostaining of TFG in human prostate cancer. Sections from paraffin-embedded tissues were subjected to antigen retrieval, followed by immunostaining with anti-TFG antibody. Non-cancerous benign epithelial hyperplastic tissues (left) show no visually detectable TFG staining, while invasive prostate cancer cells (right) show focally, but intense TFG staining. **D**: TFG mRNA expression levels in prostate cancer tissues and adjacent normal tissues (n = 29). TFG expression in prostate cancer was significantly higher than that in normal prostate tissue (Mann–Whitney U-test, $P = 0.031$, *: $P < 0.05$).

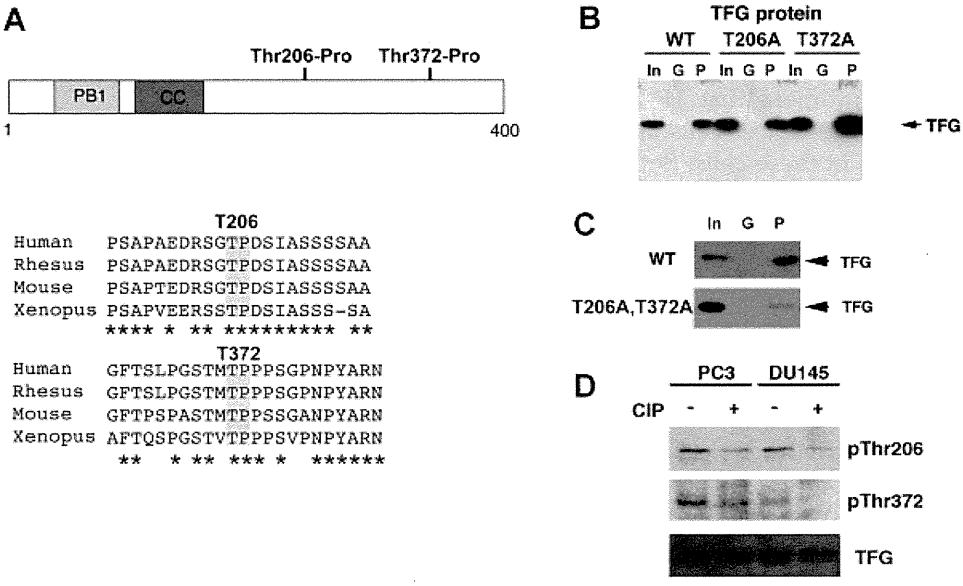

Fig. 3. TFG interacts with Pin1 via its Thr206-Pro and Thr372-Pro motifs. **A**: Schematic representation of human TFG protein (upper). Amino acid sequence alignment of the human, rhesus, mouse, and xenopus TFG proteins (lower). The conserved Thr206-Pro and Thr372 motifs are boxed. **B**: PC3 cells were transfected with the FLAG-tagged TFG (wild-type, WT) or its site-directed mutants, TFG-T206A, or TFG-T372A. At 24 hr following transfection, cell lysates were subjected to GST pull-down analysis followed by immunoblotting with anti-FLAG antibody. In, Input, G, GST; P, GST-Pin1. **C**: PC3 cells were transfected with either FLAG-tagged TFG (wild-type, WT) or its site-directed mutant on both Thr206 and Thr372 sites (T206, 372A). At 24 hr following transfection, cell lysates were subjected to GST pull-down analysis followed by immunoblotting with anti-FLAG antibody. **D**: Lysates from PC3 or DU145 cells were treated or untreated with calf-intestine alkaline phosphatase (CIP) followed by immunoblotting analysis with an anti-TFG antibody or phospho-specific antibodies targeting p-Thr206 or p-Thr372, respectively.

analysis subsequently revealed that Pin1 binds wild-type TFG and its single site-directed mutants (T206A, T372A) (Fig. 3B), but fails to interact with the corresponding TFG double mutant (2A: T206A, T372A) (Fig. 3C). These results indicate that Pin1 binds TFG on both the Thr206-Pro and Thr372-Pro motifs.

We next addressed whether Pin1 binding sites in TFG were indeed phosphorylated in prostate cancer cells. Cell lysates from PC3 and DU145 cells were treated or untreated with calf-intestine alkaline phosphatase and then subjected to immunoblotting analysis with Thr206 or Thr372 phospho-specific antibodies. We found that these two sites are indeed phosphorylated in the two prostate cancer cell lines as the signals were abolished by the pre-treatment with alkaline phosphatase (Fig. 3D). These results together indicate that Pin1 interacts with the phosphorylated Thr206 and Thr372 sites on TFG.

TFG Activates NF-kappaB in Cooperation With Pin1

A previous report has indicated that TFG binds NEMO and TANK proteins that modulate the NF-kappaB pathway and enhance NF-kappaB activity [21]. We thus speculated as to whether Pin1 enhances the function of TFG during NF-kappaB signaling. A luciferase reporter assay using the 3X kappaB-luciferase reporter construct was performed in LNCaP cells co-transfected with TFG or Pin1. Whilst the sole expression of either TFG or Pin1 had only minor effects, the co-expression of TFG and Pin1, but not its catalytic domain mutant (K63A), produced a significant increase in reporter activity (Fig. 4A). However, this is not the case in the TFG mutant lacking two Pin1 binding sites (T206A, T372A; Fig. 4B). This indicated that Pin1 promotes TFG-mediated NF-kappaB activation via its interaction with the Thr206-Pro and Thr372-Pro motifs on TFG.

TFG Promotes the Transcriptional Activity of AR

We next tested whether Pin1 enhances the transcriptional activity of androgen receptor (AR). A luciferase reporter assay using a PSA promoter containing androgen responsive elements (AREs) was performed in either LNCaP or 293T cells co-transfected with AR or TFG. Whilst the sole expression of TFG had no significant effects, the co-expression of TFG and AR produced a significant increase in the reporter activity of the PSA promoter with and without

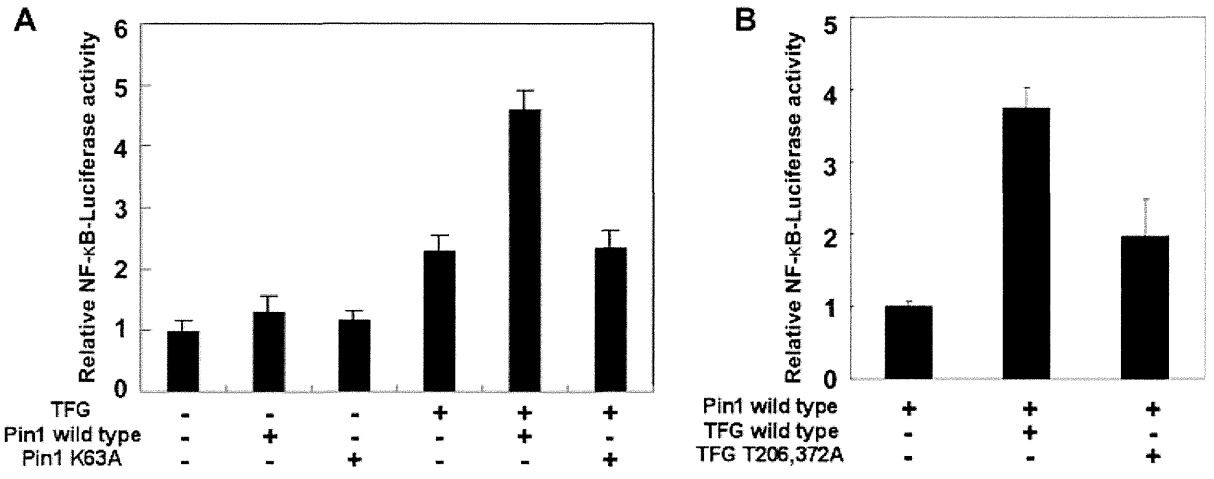

Fig. 4. Pin1 enhances TFG-mediated NF-kappaB activation. **A**, **B**: LNCaP cells were transiently transfected with the indicated plasmid vectors and co-transfected with an NF-kappaB reporter gene and pRL-TK. At 24 hr post-transfection, the cells were collected and subjected to a gene reporter assay. Immunoblots for TFG-FLAG and HA-Pin1 are shown in the upper left box. Pin1 K63A is a Pin1 mutant lacking its catalytic activity.

an AR ligand dihydrotestosterone (DHT) (Fig. 5A). Immunoprecipitation analysis revealed that TFG can specifically bind to AR (Fig. 5B). Immunofluorescent analysis further revealed that the subcellular localization of AR shifts from being cytoplasmic only to a nuclear and cytoplasmic pattern when TFG is overexpressed (Fig. 5C). These results together indicate that TFG associates with AR and thereby enhances the transcriptional activity of AR.

The Suppression of TFG Affects Cell Growth and Morphology

The above results indicated that TFG is a putative Pin1 substrate and plays an important role in oncogenicity in prostate cancer. We next addressed whether the specific depletion of TFG in prostate cancer cells has any effect on cell proliferation and tumorigenicity. For this purpose, we constructed two different siRNAs that target TFG and used the prostate cancer cell lines PC3, DU145, and LNCaP in which TFG has been shown to be highly overexpressed (Fig. 2A and B). As shown in Figure 6A, TFG protein levels were significantly reduced in cells treated with TFG-siRNAs when compared with control siRNA treated cells.

We next evaluated the effects of TFG depletion on in vitro cell growth and morphology. The suppression of TFG resulted in a substantially decreased cell growth (Fig. 6B). Morphological analysis also revealed that cells expressing TFG-siRNAs were relatively larger and contained vacuolated nuclei and a granular cytoplasm, thus showing specific features of senescent cells. Senescence-associated beta galactosidase staining (SABG) of these cells further revealed significant increases in the number of SABG-positive cells in the TFG-siRNA population, but not in the control siRNA cells (Fig. 6C and D). These results indicate that the loss of TFG expression affects both cell proliferation and morphology by partly inducing cellular senescence in prostate cancer cells.

The Association Between TFG Expression and Prostate Cancer Recurrence

We next investigated the relationship between TFG expression levels and cancer recurrence. The Kaplan–Meier Method and log rank test were used to compare the significance of the recurrence free curves between two groups among 29 prostate cancer samples taken from patients after a radical prostatectomy. The results indicated a strong association between TFG expression and tumor recurrence (Fig. 7A). However, there were no such association between cancer recurrence and age, pre-operative PSA, Gleason score, or UICC stage (Fig. 7B–E). These relationships were also confirmed using the multi-variate analysis between the TFG expression levels and recurrence-free survival times (Table II).

We also investigated the relationship between TFG expression level and Age, Pre-operative PSA, Gleason score, or UICC stage among 29 prostate cancer samples taken from patients after prostatectomy (Fig. 8). There was no significant relevance between TFG expression levels and these parameters. These results demonstrate that TFG expression in prostate cancer tissues may predict a high risk of recurrence after a prostatectomy.